ELSEVIER

Journal of Structural Geology 29 (2007) 950–960

JOURNAL OF STRUCTURAL GEOLOGY

www.elsevier.com/locate/jsg

An analytical solution in 2D for the motion of rigid elliptical particles with a slipping interface under a general deformation

Kieran F. Mulchrone*

Department of Applied Mathematics, National University of Ireland, University College, College Road, Cork, Ireland

Received 23 August 2006; received in revised form 1 March 2007; accepted 4 March 2007
Available online 14 March 2007

Abstract

A mathematical model for rigid inclusions with a slipping interface immersed in a general 2D homogeneous deformation is developed. Under bulk pure shear inclusions are expected to rapidly approach the stretching axis when compared to the behaviour of inclusions with no slip at the interface. The derived model predicts synthetic and antithetic motion into a stable orientation under simple shear, and thereafter the inclusion makes an antithetic angle with the shear direction. Under simple shear rotation rates can be higher or lower than those of no-slip inclusions, depending on orientation. A direct relationship between object inclination to the shear direction and the vorticity of the bulk flow is predicted. The model compares well with published analogue and numerical experiments.

Keywords: Slipping interface; Antithetic rotation; Stable direction; Ellipse

1. Introduction

Natural rocks deform in very complex ways. Reliable estimates of finite strain and the kinematic vorticity number (W_k) or flow type are a key part of understanding local and regional rock deformation (see Xypolias and Koukouvelas, 2001 for an example study). A plethora of methods exist for finite strain estimation (see Mulchrone et al., 2003 and references therein), however, these rely largely on the assumption of passive behaviour (i.e. elliptical inclusions behave exactly like the enclosing matrix) and give no information about the kinematics of deformation. Over the last 20 years or so there has been a considerable research effort put into understanding porphyroclast systems (Passchier and Simpson, 1986) because they may be the source of kinematic and mechanical information (Bose and Marques, 2004). The mathematical model of Jeffery (1922) for the behaviour of a rigid ellipsoid immersed in a Newtonian fluid with no slip at the boundary has provided the theoretical basis for much of this work and was introduced to the structural geology literature by Ghosh and Ramberg (1976). More recently researchers have begun to consider different models for inclusion behaviour: (i) rigid with no-slip (Jeffery, 1922; Mushhelishvili, 1953; Mason and Manley, 1957; Bretherton, 1962; Ghosh and Ramberg, 1976; Freeman, 1985; Passchier, 1987; Jezek et al., 1999; Arbaret et al., 2001; Mandal et al., 2001; Schmid, 2002; Marques and Coelho, 2003), (ii) rigid with slip on the boundary (Ildefonse and Mancktelow, 1993; Odonne, 1994; Kenkmann and Dresen, 1998; Pennacchioni et al., 2000; Mancktelow et al., 2002; Schmid and Podladchikov, 2003, 2004; Samanta and Bhattacharyya, 2003; Ceriani et al., 2003; Bose and Marques, 2004; Marques and Bose, 2004; Marques et al., 2005a), (iii) rigid with slip and/or no-slip in confined flow (Marques and Coelho, 2001; Taborda et al., 2004; Marques et al., 2005b), (iv) non-rigid with no-slip (Eshelby, 1957; Bilby and Kolbuszewski, 1975; Schmid and Podladchikov, 2003; Mulchrone and Walsh, 2006). In this paper a 2D analytical solution is derived for the case of a rigid object immersed in a Newtonian fluid with slip at the boundary. After a brief review of related work, the solution is presented.

* Tel.: +353 21 4903411; fax: +353 21 4271040.
E-mail address: k.mulchrone@ucc.ie

0191-8141/$ - see front matter © 2007 Elsevier Ltd. All rights reserved.
doi:10.1016/j.jsg.2007.03.008

Mantled porphyroclasts have been the subject of analogue modelling (Passchier and Sokoutis, 1993; Passchier et al., 1993; ten Brink and Passchier, 1995) and experimental results support a direct relationship between rheology and developed mantle structures (i.e. stress sensitivity). Theoretical and numerical studies of deflections around rigid spherical inclusions have also been conducted (Masuda and Mizuno, 1995, 1996a,b) for both Newtonian and non-Newtonian enclosing materials which indicated that it was the initial size of the mantle rather than the stress sensitivity which determined the type of mantle structure developed. Bons et al. (1997) showed that the applied boundary conditions (i.e. simple shear at an infinite versus a finite distance) determine the type of flow pattern around a rigid inclusion (i.e. eye-shaped or bow-tie-shaped separatrix, Passchier et al., 1993) and thus the mantle structure developed. Stress sensitivity was found to be of secondary importance. Mandal et al. (2001) demonstrated that a bow-tie separatrix can develop under combined simple and pure shear. Bose and Marques (2004) presented the results of analogue models suggesting that slip or no-slip at inclusion boundaries is an important factor in determining the morphology of mantle structures, as well as the flow pattern in the matrix, mantle rheology and the mantle position with respect to the separatrix. In a numerical study, Marques et al. (2005a) demonstrated the existence of cats eyes-shaped flow under the influence of a low viscosity layer between the matrix and inclusion. However, Schmid and Podladchikov (2005) used a three-phase finite-element model with power-law rheologies to investigate an isolated mantled porphyroclast in simple shear. They were able to produce gauges for effective mantle/matrix viscosity contrast, production rates of mantle material as a function of bulk shear strain and the total shear strain.

Populations of rigid inclusions have been the subject of theoretical (Fernandez et al., 1983; Fernandez, 1987; Passchier, 1987; Masuda et al., 1995; Marques and Coelho, 2003), experimental (Ildefonse et al., 1992a,b; Arbaret et al., 1996; Herweg and Handy, 1998) and natural study (Manga, 1998; Pennacchioni et al., 2001). In the case of populations of non-interacting particles (Fernandez et al., 1983; Fernandez, 1987; Masuda et al., 1995; Marques and Coelho, 2003) with no-slip at the boundary (Jeffery, 1922), pulsating fabrics have been predicted under simple shear although the period of a fabric cycle increases with inclusion aspect ratio. Interaction of particles (Ildefonse et al., 1992a,b; Arbaret et al., 1996) affects the behaviour of populations as revealed in analogue experiments. The development of pulsating fabrics is inhibited and the fabric remains at a small angle to the shear plane. Samanta et al. (2003) demonstrated theoretically and experimentally that for interacting spherical particles rotation rates are retarded.

In the vast majority of research no-slip boundary conditions are assumed, however, theoretical and experimental studies suggest that slip on the boundary between the inclusion and the matrix could significantly influence the behaviour of inclusions (Ildefonse and Mancktelow, 1993; Odonne, 1994; Kenkmann and Dresen, 1998; Pennacchioni et al., 2000; Mancktelow et al., 2002; Schmid and Podladchikov, 2003, 2004; Samanta and Bhattacharyya, 2003; Ceriani et al., 2003; Marques and Bose, 2004; Marques et al., 2005a,b). Ildefonse and Mancktelow (1993) observed increased inclusion rotation rates under simple shear but reduced rates under pure shear. Additionally, under simple shear they reported that inclusions rotated towards the shear plane and remained there. Due to modification of the soap layer used to facilitate slip, this conclusion is only valid for low finite strains. Furthermore, they found that because the inclusion does not rotate through the shear plane δ-type mantle structures will not develop. Odonne (1994) carried out analogue modelling of a deformable inclusion and found that with a high degree of bonding the inclusion deforms whereas as the level of bonding decreases the inclusion effectively behaves in a rigid manner. Marques and Coelho (2001) experimentally investigated the effect of simple shear applied at a finite distance on the behaviour of an isolated rigid inclusion and found that it departs quite significantly from that under simple shear applied at infinity and when the interface coupling is reduced antithetic rotation is possible. Mancktelow et al. (2002) performed ring shear experiments to investigate the effect of boundary slip or no-slip on differently shaped inclusions. Elliptical shapes with slip showed reduced rotation rates when the long axis is close to the shear plane, however, rhomboidal shapes with slip attained stable orientations with their long sides subparallel to the shear plane and back rotation (opposite to the bulk sense of shear) was also observed. In the case of no-slip, inclusions essentially behaved as predicted by the theory of Jeffery (1922). Ceriani et al. (2003) also describe antithetic rotation for elliptical inclusions and metastable positions for a lubricated interface. Metastable positions may be due to changing thickness of the layer of lubrication during deformation. In general, the presence of a lubricating mantle zone produces faster rotation rates than that predicted by the no-slip theory. Schmid and Podladchikov (2003) developed analytical solutions for the case of a deformable circular inclusion with a weak rim and have shown it may effectively be considered as a weak inclusion. Samanta and Bhattacharyya (2003) considered modes of detachment at a rigid-inclusion–matrix interface by calculating the stresses acting on the interface using Jeffery's (1922) theory (i.e. no-slip). They then studied the occurrence of detachments by initiating detachment once selected tensile and shear strengths had been exceeded. However, they did not investigate the influence of such detachments on the dynamics of clast behaviour. Bose and Marques (2004) and Marques and Bose (2004) reported on the results of precision experiments dealing with rigid inclusions composed of ice with slip on the boundary. There were clear differences between the behaviour of inclusions with slip and theoretical and experimental results for the no-slip case. In addition, they found antithetic rotation into a stable orientation which depends on aspect ratio and shape and also the occurrence of a metastable orientation separating the synthetic and antithetic rotational fields. A numerical study by Marques et al. (2005a), in which a low viscosity layer was placed between the matrix and inclusion, found close

agreement with analogue experiments. Schmid and Podladchikov (2004) made the equivalent void conjecture to explain the common observation of stable and metastable clast inclinations in shear zones. This approach assumes that the mantle material around a rigid clast is significantly weaker than the surrounding matrix, which effectively isolates the rigid clast from the matrix. Furthermore, it is asserted that the combined rigid inclusion/weak mantle package behaves as an area preserving void whose shape changes little due to the presence of the rigid inclusion.

It is clear that structures developed in and around rigid objects immersed in a viscous fluid have greatly aided our ability to understand deformation (Passchier and Trouw, 1996, pp. 116–121). However, as indicated above, recent analogue modelling and natural studies on porphyroclasts have cast doubt on the ubiquitous applicability of rigid no-slip models to explain clast behaviour (for example Ceriani et al., 2003; Pennacchioni et al., 2001; Bose and Marques, 2004; Marques and Bose, 2004; Marques et al., 2005a). Pennacchioni et al. (2001) and Schmid and Podladchikov (2004) pointed out that there are no models in existence which can explain the natural data that they have collected. It is also noticeable that most of the analogue studies make comparisons with Jeffery's (1922) theory, which does not even consider slipping on the interface.

With these factors as motivation, a solution is derived for slipping rigid objects immersed in a general homogeneous deformation. The resulting model should be of use in understanding natural porphyroclast systems and provide a theoretical framework better matched to experimental results. To the best of our knowledge, this solution has not been derived previously (although Schmid and Podladchikov, 2003 do consider the effect of weak rim on a circular inclusion and Samanta and Bhattacharyya, 2003 consider interface detachments) and is of direct relevance to the understanding of rock deformation. The solution is explored in some detail below and a full derivation is given in the Appendix. Finally, a vorticity gauge based on the model is proposed.

2. Guide to the model

The solution developed here is ultimately based on the solution for a rigid object immersed in a viscous fluid by Jeffery (1922) and the extension to deformable inclusions of Mulchrone and Walsh (2006), however, it differs quite significantly from Jeffery's (1922) approach in the way velocities and stresses are handled and equated at the boundary. A detailed derivation is presented in the appendices. The rotational convention adopted here is that the direction along the positive x-axis is 0° and that anti-clockwise is the positive direction. At any time instant the model consists of a non-rigid elliptical object of viscosity μ_i immersed in a matrix of viscosity μ_e whose long axis makes an angle ϕ with the positive x'-direction (see Fig. 1) and whose long and short axes are a and b, respectively. The viscosity ratio is defined as $\mu_r = \mu_e/\mu_i$ and the ellipse axial ratio $R = a/b$. The (x', y') coordinate system is fixed whereas the (x, y) coordinate system is always defined with respect to the long and short axes of the elliptical object. In the absence of the elliptical object, an homogeneous deformation defined by a given velocity gradient tensor ($\mathbf{L}'$) with respect to (x', y') prevails. In the presence of the elliptical object, the homogeneous deformation is perturbed near the elliptical object, but at large distances from the object this perturbation disappears. Furthermore, we assume that inside the elliptical object a general homogeneous deformation occurs (i.e. no perturbation) which is usually different from the unperturbed external deformation. This guarantees that the elliptical object maintains an elliptical shape at all times.

The derivation proceeds by assuming a form for the perturbed flow velocity field (u, v) in terms of functions which firstly solve Laplaces equation (i.e. for a function f, $\nabla^2 f = 0$) and secondly vanish far from the elliptical object. Slip on the boundary is allowed by continuity/equality of normal velocities and stresses at the ellipse boundary. In addition, shear stresses at the boundary are set to zero and no restrictions are imposed regarding continuity of internal and external boundary parallel velocities. The external velocity field can be written in terms of the internal velocity field, the unperturbed flow, and the instantaneous shape of the ellipse (see Eqs. (14) and (15)). Using the solution for the external velocity field and the assumed internal velocity field both the internal and external stresses can be calculated. Imposing stress boundary conditions the remaining unknown parameters for the internal velocity field can be calculated (see Eq. (24)). Therefore, the internal and perturbed velocity fields are all known and the problem is solved. As shown in the Appendix, the solution is only valid for two special cases (i) a perfectly rigid object and (ii) an area preserving void. From now on the paper concentrates on the case of a rigid object.

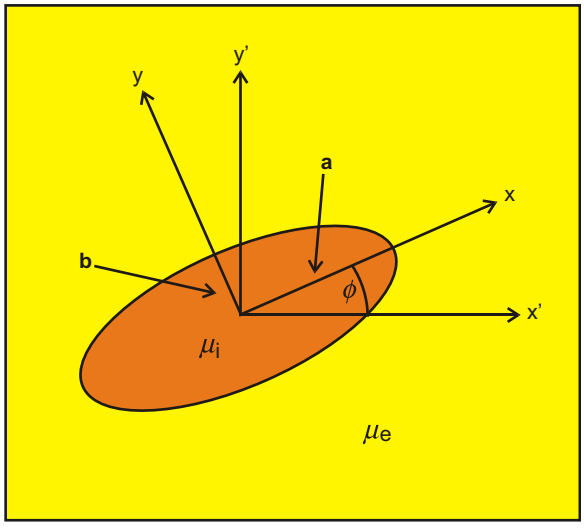

Fig. 1. Setting for the problem. An elliptical inclusion with viscosity μ_i is enclosed in a medium with viscosity μ_e and has long and short semi-axes labelled a and b, respectively. There is a fixed coordinate system (x', y') and a coordinate system which remains parallel to ellipse axes denoted by (x, y).

3. Model behaviour

In this section, the dynamics of the derived solution is examined in the context of typical structural geological flow-types. In exploring the solution it makes sense to make comparisons with the no-slip solution of Mulchrone and Walsh (2006). In the text below subscript s refers to the slipping case whereas subscript ns refers to no-slip. In general, the rotation rate for a slipping ellipse is:

$$\left.\frac{\mathrm{d}\phi}{\mathrm{d}t}\right|_{\mathrm{s}} = \frac{1}{2}\left(L'_{21} - L'_{12}\right) + \frac{(R+1)\left(\left(L'_{21}+L'_{12}\right)\cos 2\phi - 2L'_{11}\sin 2\phi\right)}{2(R-1)} \quad (1)$$

For the no-slip case (and a rigid inclusion) the rotation rate is (Mulchrone and Walsh, 2006):

$$\left.\frac{\mathrm{d}\phi}{\mathrm{d}t}\right|_{\mathrm{ns}} = \frac{1}{2}\left(L'_{21} - L'_{12}\right) + \frac{\left(R^2-1\right)\left(\left(L'_{12}+L'_{21}\right)\cos 2\phi - 2L'_{11}\sin 2\phi\right)}{2\left(1+R^2\right)} \quad (2)$$

The relative rotation rate $(\mathrm{d}\phi_{\mathrm{r}}/\mathrm{d}t)$ is obtained by dividing Eq. (1) by Eq. (2).

3.1. Bulk pure shear

For bulk pure shear (setting $L'_{12} = L'_{21} = 0$) the rotation rates are characterised as follows:

$$\left.\frac{\mathrm{d}\phi}{\mathrm{d}t}\right|_{\mathrm{s}} = -\frac{(R+1)L'_{11}\sin 2\phi}{(R-1)}$$
$$\left.\frac{\mathrm{d}\phi}{\mathrm{d}t}\right|_{\mathrm{ns}} = -\frac{\left(R^2-1\right)L'_{11}\sin 2\phi}{\left(R^2+1\right)} \quad (3)$$
$$\frac{\mathrm{d}\phi_{\mathrm{r}}}{\mathrm{d}t} = \frac{\left(R^2+1\right)}{(R-1)^2}$$

from analysis $(\mathrm{d}\phi_r/\mathrm{d}t)>1$ always, meaning that slipping ellipses always rotate faster than no-slip ellipses. By setting $\mathrm{d}\phi/\mathrm{d}t|_{\mathrm{s}} = 0$ in Eq. (3) it is found that the rotation rate is 0 at $\phi = n\pi/2$, where n is 0 or a positive integer. The dynamics of the situation is illustrated in Fig. 2. For $L'_{11} > 0$, there is a stable fixed point (i.e. an orientation that ellipses tend to rotate towards) at $\phi = 0$ and an unstable fixed point at $\phi = \pi/2$. This is identical to the dynamics of rigid and non-rigid no-slip ellipses (and indeed passive lines under the March model, March, 1932) in pure shear flow. The main difference between the models is relatively faster rates of rotation for slipping interfaces (see Fig. 3).

3.2. Bulk simple shear

The rotational dynamics of slipping objects under bulk simple shear is quite different from that predicted by previous theories of no-slip objects i.e. Jeffery (1922). For bulk simple shear, the rotation rates are characterised as follows:

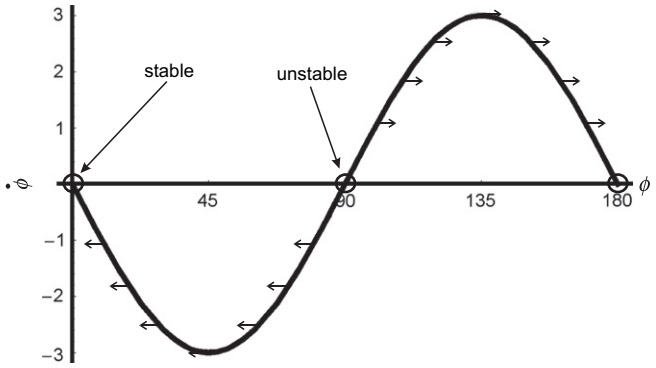

Fig. 2. Dynamics of pure shear rotation. Stable orientation coincides with the stretching axis.

$$\left.\frac{\mathrm{d}\phi}{\mathrm{d}t}\right|_{\mathrm{s}} = \frac{1}{2}L'_{12}\left(\frac{(R+1)\cos 2\phi}{R-1} - 1\right)$$
$$\left.\frac{\mathrm{d}\phi}{\mathrm{d}t}\right|_{\mathrm{ns}} = \frac{1}{2}L'_{12}\left(\frac{\left(R^2-1\right)\cos 2\phi}{\left(R^2+1\right)} - 1\right) \quad (4)$$

It is not possible to write a simplified rotation rate ratio in this case.

Letting the rotation rates in Eq. (4) go to zero, we can find the fixed or stable positions. For slip we find that these occur for:

$$\phi^*_{\mathrm{s}} = \pm\frac{1}{2}\cos^{-1}\left(\frac{R-1}{R+1}\right) \quad (5)$$

which depends only on the axial ratio and in the case of no-slip:

$$\phi^*_{\mathrm{ns}} = \pm\frac{1}{2}\cos^{-1}\left(\frac{R^2+1}{R^2-1}\right) \quad (6)$$

However ϕ^*_{ns} is complex for $R > 1$, so no fixed points exist and the objects tend to rotate continuously. By contrast ϕ^*_{s} is real for $R > 1$ therefore under slip objects tend to rotate into one of these fixed positions. The dynamics of this situation is illustrated in Fig. 4a and shows the presence of two fixed points, one stable and one unstable in the case of a slipping ellipse. The orientation of the fixed positions can be calculated

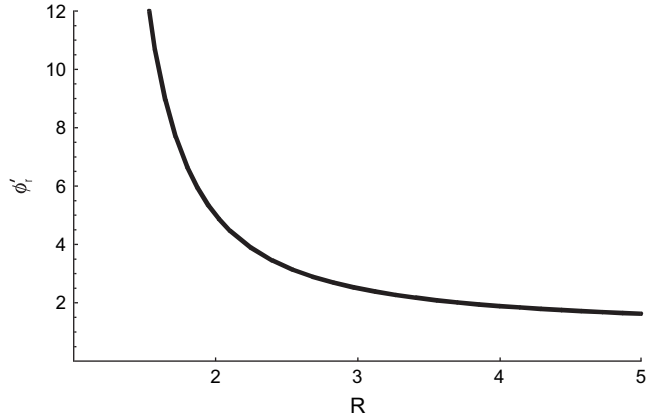

Fig. 3. Relative rotation rate $(\phi'_r = \mathrm{d}\phi_r/\mathrm{d}t)$ of inclusion with slip at the interface versus an inclusion with no-slip as a function of axial ratio (R) under bulk pure shear.

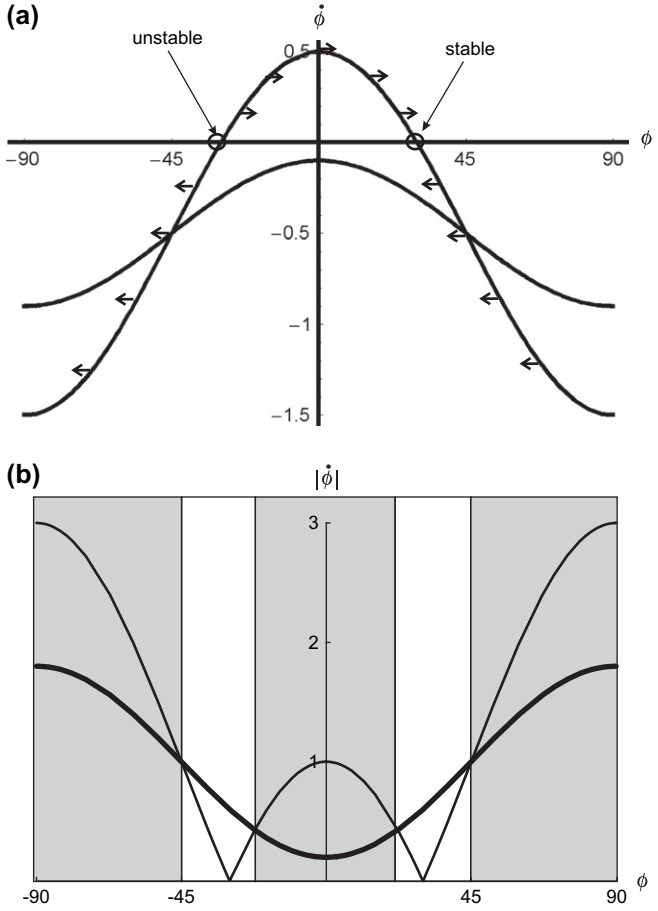

Fig. 4. Bulk kinematics is simple shear. (a) Stability diagram for a rigid object ($R = 3$) with a slipping interface (curve with arrows on) as compared with a rigid object with no slip at the interface which rotates synthetically continuously. (b) Plot of absolute rotation rates (thick line represents inclusion with no-slip, thin line inclusion with slip), illustrating shaded regions where the inclusion with slip rotates faster and unshaded regions where it rotates slower.

from Eq. (5). It is also clear that (see Fig. 4b) the magnitude of the rotation rates in the case of slip may be much larger than those in the no slip case, however, near the stable points the absolute rate of rotation in the slip case is lower. This indicates that ellipses will tend to rotate into regions around the fixed position relatively quickly and then slowly (as compared to the no-slip case) attain the stable position. The relationship between the orientation of the stable fixed position and axial ratio is given in Fig. 5. In the no slip case the object is predicted to continuously rotate negatively (i.e. synthetically). Another important feature of the slip model presented here is that antithetic rotation into the stable direction is permitted. This is in agreement with the results of analogue experiments on lubricated rigid elliptical particles under simple shear (Ildefonse and Mancktelow, 1993; Odonne, 1994; Kenkmann and Dresen, 1998; Pennacchioni et al., 2000; Mancktelow et al., 2002; Schmid and Podladchikov, 2003, 2004; Samanta and Bhattacharyya, 2003; Ceriani et al., 2003; Bose and Marques, 2004; Marques and Bose, 2004; Marques et al., 2005a).

Fig. 6 illustrates the relative rotation rates of slip against no slip rigid objects. Within the relative rotation rate range of

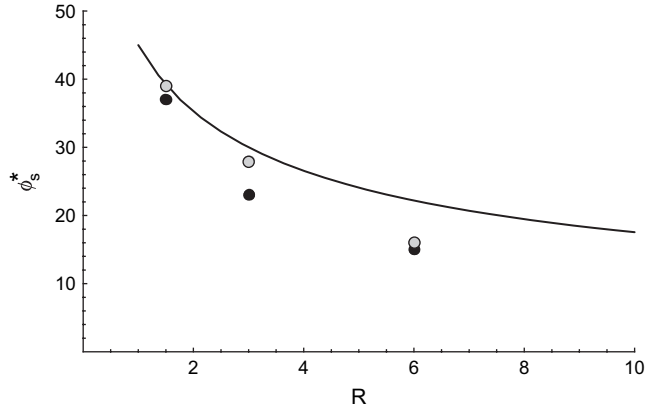

Fig. 5. Curve of stable direction versus axial ratio under bulk simple shear. Filled black points are taken from the experimental results of Marques and Bose (2004) for the stable orientation attained by a rigid ellipse with a slipping interface under simple shear whereas the filled grey points correspond to the numerical results of Marques et al. (2005a).

$(-1, 1)$ slipping interface objects rotate more slowly than their no-slip counterparts. Moreover, at orientations greater than $\pm 45°$ the converse is true. Notice also that negative relative rotation rates occur close to the 0° direction indicating the antithetic motion of slip ellipses compared with the always synthetic rotation of no-slip ellipses.

4. Vorticity analysis

The solution derived in this paper has potentially many applications and in this section a simple application to vorticity analysis is presented. Vorticity is a measure of the degree of

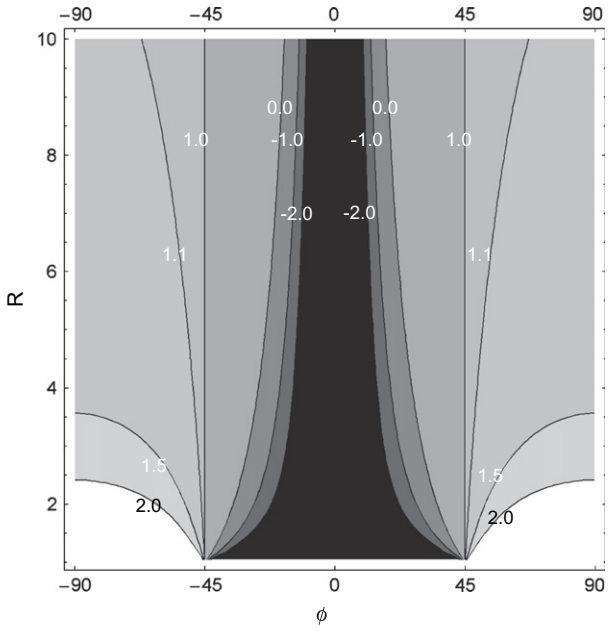

Fig. 6. Contour plot of relative rotation of slip compared with no slip for rigid objects as a function of axial ratio and orientation under simple shear. Numbers indicate relative rotation rates.

non-coaxiality in a particular flow (Means et al., 1980; Ghosh, 1987) and the kinematic vorticity number (W_k) varies from 0 (pure shear) to 1 (simple shear) and beyond for rotationally dominated flows. Ghosh and Ramberg (1976) and Marques and Coelho (2003) investigated the stable directions for rigid objects with no slip at the boundary (Jeffery's, 1922 model). A commonly used general deformation scenario used in geological analysis is where simple shear and pure shear are combined as follows:

$$L' = \begin{pmatrix} L'_{11} & L'_{12} \\ 0 & -L'_{11} \end{pmatrix} \tag{7}$$

where positive L'_{11} is transpressive and negative L'_{11} is transtensional. From Eq. (1), the rotation rate is given by:

$$\left.\frac{\mathrm{d}\phi}{\mathrm{d}t}\right|_s = -\frac{1}{2}L'_{12} + \frac{(R+1)\left(L'_{12}\cos 2\phi - 2L'_{11}\sin 2\phi\right)}{2(R-1)} \tag{8}$$

In this more general case, the position of the fixed points is derived by setting the rotation rate to 0 and solving for ϕ to give:

$$\phi_s^* = \mathrm{Re}\left[-\frac{1}{2}i\log\left(\frac{iL'_{12}(R-1) \pm 2\sqrt{L'^2_{12}R + L'^2_{11}(R+1)^2}}{\left(2L'_{11} - iL'_{12}\right)(R+1)}\right)\right] \tag{9}$$

The relationship between ϕ_s^* and the kinematic vorticity number (W_k) is illustrated in Fig. 7. This clearly indicates that the stable orientation obtained by a slipping elliptical object and its axial ratio can be used to estimate the kinematic vorticity number. It is important to note that the accuracy of an estimate based on a single observation will not be high, however, more exact methods based on populations can be developed.

5. Comparing deformation patterns around slip and no-slip inclusions

It is beyond the scope of this paper to provide a detailed analysis of deformation patterns around slipping ellipses, however, it is instructive to consider the special case of a rigid object in simple shear flow. Fig. 8 presents the results of two simulations with identical starting positions (i.e. $R = 2.5$, $\mu_r = 0$ and an initial orientation of $\phi = -10°$), however, the left hand diagrams are for slip whereas the right hand are for no-slip. The relevant equations for the motion of grid points inside and outside the inclusion (derived here and in Mulchrone and Walsh, 2006) were solved in Mathematica and by keeping track of connections the deformed grid was generated.

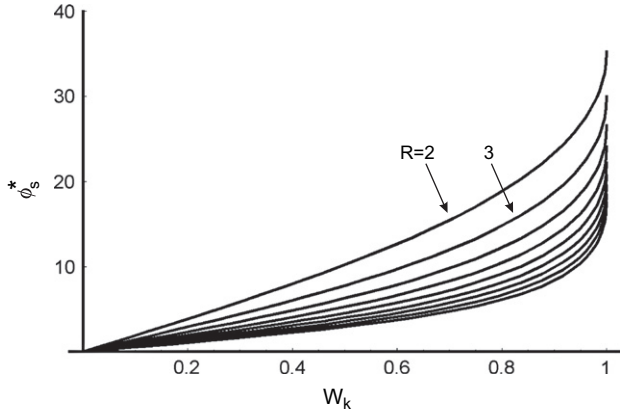

Fig. 7. Relationship between stable direction and flow type (W_k).

The relative rapidity of the rotational phase of slip motion is nicely exemplified where, at the relatively low finite strain of $R_s = 2.62$, where R_s is the axial ratio of the finite strain ellipse, the slip ellipse has almost antithetically rotated into the stable orientation (approximately 20°). By contrast the no-slip ellipse has synthetically rotated through $-10°$ in the same interval. There are some remarkable differences between deformation patterns around the inclusions in the two cases. At relatively moderate simple shear ($R_s = 17.94$, $\gamma = 6$), the no slip inclusion has a more smoothly varying pattern around it, with low deformation zones adjacent to the long axis ends making a pattern akin to an σ-structure (Passchier and Simpson, 1986). In contrast the no-slip inclusion displays a more varied deformation pattern with high deformation zones emanating from the long axis ends crossing the median line akin to a δ-structure (Passchier and Simpson, 1986) or more strictly because $R > 1$ a rolling structure (Van Den Driessche and Brun, 1987).

6. Discussion and conclusions

Some analogue experiments on the behaviour of rigid elliptical objects with lubricated boundaries have been reported relatively recently in the literature (Ildefonse and Mancktelow, 1993; Marques and Cobbold, 1995; Marques and Coelho, 2001; Mancktelow et al., 2002; Ceriani et al., 2003; Marques and Bose, 2004; Marques et al., 2005a). As shown in Table 1 all related analogue and theoretical results predict antithetic rotation of inclusions, stable orientations and poor correlation with the model Jeffery (1922). Ildefonse and Mancktelow (1993) used rigid rectangular objects in both pure and simple shear deformation experiments, although rectangular objects may approximate elliptical objects, it is clear that differences arise due to morphology (e.g. Marques and Bose, 2004; Marques et al., 2005a). They found increased relative rotation rates under pure shear but the converse for simple shear. This is consistent with the predictions of the present model i.e. increased rotation rates for pure shear and both decreased and increased rotation rates in simple shear (see Figs. 3 and 4). In their experiments Marques and Cobbold (1995) found antithetic rotation into a fixed/stable orientation, however, they focused more on the development of folds adjacent to inclusions. Marques and Coelho (2001) also looked at a slipping interface but additionally included finite shear zone width (a factor not included in the present model). However, they found antithetic rotation and experimental results are similar to the simulations presented in Fig. 8. Mancktelow et al. (2002) motivated by the absence of Jeffery's transient fabrics in natural shear zones, experimentally studied the influence of interface slip on particle motion. They found that a slipping particle tends to initially stabilise for shear strains below 10, but then tends to continuously rotate. This may be due to the experimental set

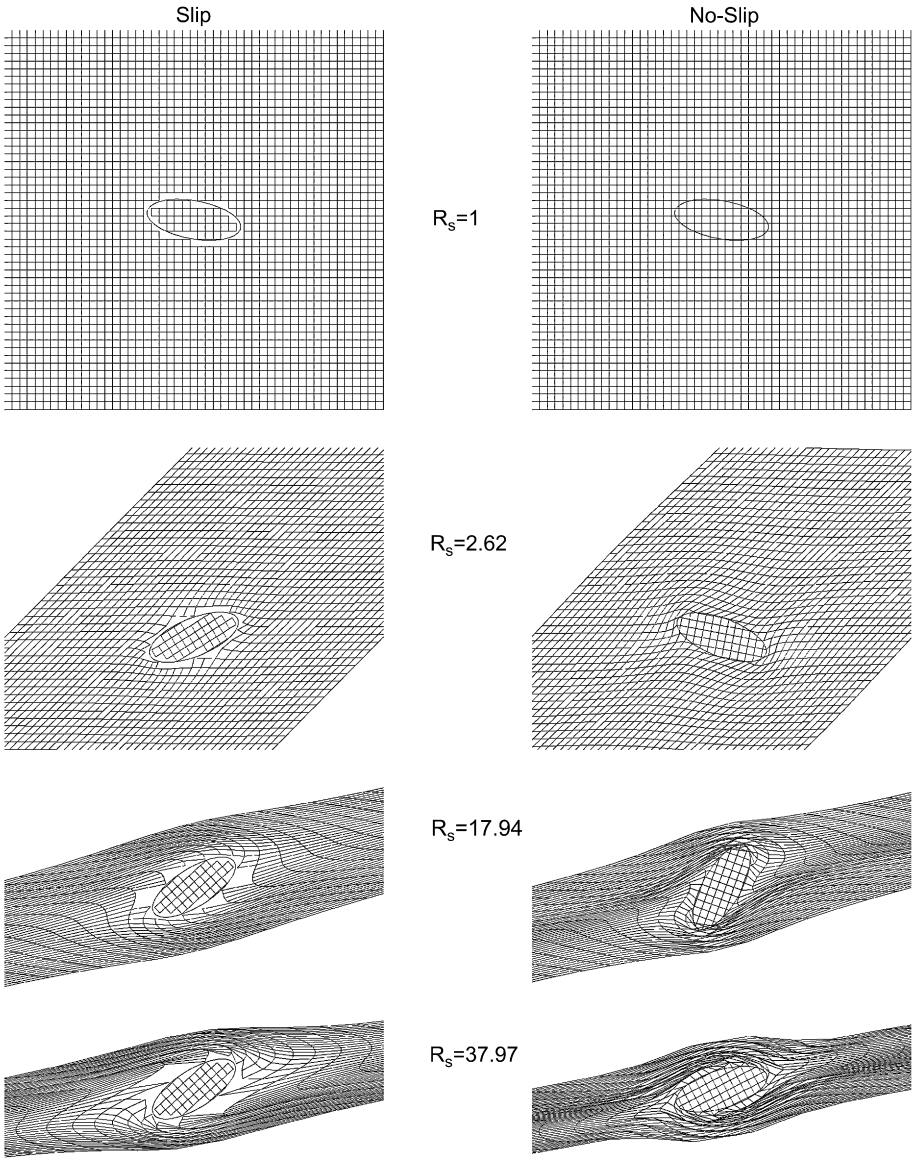

Fig. 8. Simulation of grid deformation during a slipping model and the traditional no-slip model.

up whereby the lubricant thins as deformation progresses, although Marques and Bose (2004) eliminated this factor in their experimental set up by using ice inclusions. Monoclinic rhomboidal particles were found to attain a stable position. Ceriani et al. (2003) found antithetic rotation into a metastable position of 16° (my rotation convention). Absolute agreement between experimental observations and the model derived here is not expected because of the way in which the slipping

Table 1
Experimental results on inclusions with slip on the boundary

Study	Experimental details	Lubricant	Antithetic rotation	Stable orientation	Deviation from Jeffery (1922)
Marques and Coelho (2001)	Confined, simple shear, slip and no-slip	Liquid soap	Yes	20°	Yes
Mancktelow et al. (2002)	Couette flow, slip and no-slip	Liquid soap	Yes	5–20°	Yes
Ceriani et al. (2003)	Couette flow, slip and no-slip	Liquid soap	Yes	Not attained	Yes
Marques and Bose (2004)	Simple shear, slip	Ice	Yes	See Fig. 5	Yes
Marques et al. (2005a)	Simple shear, slip	Low viscosity layer	Yes	See Fig. 5	Yes

Typical features (antithetic rotation, stable orientation and deviations from the no-slip model of Jeffery, 1922) are also exhibited by the analytical solution derived here.

interface is modelled. It is difficult to experimentally maintain the theoretical boundary conditions imposed here. However, there is broad agreement between the theory presented here and experiment. Marques and Bose (2004) overcame the experimental limitation of an ephemeral boundary by using ice in experiments. They found both antithetic and synthetic rotation and the presence of stable and meta-stable orientations in broad agreement with the predictions of the present analytical model. Furthermore the stable orientations compare favourably with the predicted orientations derived here (Fig. 5) and vary in a similar manner with axial ratio. Absolute agreement has not been found possibly due to the migration of liquid water into tail regions around the clast, a feature not present in the derived model. The numerical model of Marques et al. (2005a), where the interface slip is provided by a low viscosity layer between the inclusion and matrix, provides similar results. Again absolute agreement between the numerical model and analytical model is not found (Fig. 5), however, the boundary conditions applied are different.

Pennacchioni et al. (2001) postulate stablisation of porphyroclasts in natural shear zones, however, the average orientations are 6–10° with the shear direction which is considerably less than that predicted for individual objects in the model developed here. Perhaps this is due to non-zero shear stresses across boundaries in nature because of the enormous pressures under which these structures evolve. There are additional differences between the natural inclusions and behaviour predicted by the model derived here. For example, Pennacchioni et al. (2001) found that the stabilisation direction is independent of the aspect ratio whereas in the model there is a direct relationship predicted (see Fig. 5). Furthermore, low aspect ratio particles failed to attain a stable orientation, a feature which cannot be explained by the slip model.

A model for the motion of rigid elliptical inclusions in a generally deforming linear viscous fluid with slipping interfaces has been derived. Although there are certain features of both natural and experimental studies which the model does not explain, it appears to successfully replicate many features first noted in analogue experiments such as antithetic rotation, stable particle positions and rotation rates different to those predicted by no-slip models.

Acknowledgements

This work was partially funded by the Science Foundation Ireland research frontiers program (grant 04/BR/ES0020). Many thanks to Dr. Dani Schmid and Dr. Georgio Pennacchioni who reviewed an earlier version of this manuscript. Dr. Schmid pointed out a fatal flaw in the original analysis and Dr. Pennacchioni highlighted ways in which the manuscript could be made more geologically relevant and helped refine some of the interpretations. Further reviews by Dr. Schmid and Dr. F.O. Marques have substantially improved the final version. Thanks also to Prof. Cees Passchier for editorial help.

Appendix

The approach to finding the solution to the problem of both rigid and non-rigid ellipses with slip at the interface in a viscous fluid is similar to that taken by Mulchrone and Walsh (2006). To conserve space the reader is referred first to the appendices of Mulchrone and Walsh (2006) and references to equations from that paper are prefixed by MW. Eqs. (MW16)–(MW48) apply equally in the present case and the assumed form of the perturbed velocity field outside the ellipse (Eqs. (MW47)–(MW55)) is also identical. The assumed form of the internal motion differs and is given by:

$$u_\mathrm{i} = k_1 x + \omega_1 y \tag{10}$$

$$v_\mathrm{i} = -\omega_2 x - k_2 y \tag{11}$$

meaning that the object can rotate and deform homogeneously as well as gain or loose volume if $k_1 - k_2 \neq 0$. At the surface of the ellipse (i.e. $l = 0$) the internal and external velocities must agree, however, as slip is allowed it is only the boundary normal components of velocity that must agree. The unit normal vector ($\mathbf{n}$) to the boundary of the ellipse is calculated using the gradient (Marsden and Tromba, 2003, p. 170):

$$\mathbf{n} = P\begin{pmatrix} \dfrac{x}{a^2} \\ \dfrac{y}{b^2} \end{pmatrix} \tag{12}$$

so that taking both the internal and external velocity components projected along $\mathbf{n}$ the velocity boundary condition is (see Marsden and Tromba, 2003, p. 31):

$$\frac{\mathbf{n}\cdot\mathbf{v}_\mathrm{i}}{\|\mathbf{n}\|^2}\mathbf{n} = \frac{\mathbf{n}\cdot\mathbf{v}_\mathrm{e}}{\|\mathbf{n}\|^2}\mathbf{n} \tag{13}$$

where $\mathbf{v}_\mathrm{i} = (u_i, v_i)$ is the internal velocity vector and $\mathbf{v}_\mathrm{e} = (u, v)$ is the external velocity vector. Eq. (13) is satisfied by equating like coefficients to give the following set of equations:

$$\begin{aligned}
&2A(\alpha_0 + \beta_0) + k_1 - L_{11} - \gamma_0 W = 0 \\
&\begin{bmatrix} b^2(2\beta_0 H - 2\alpha_0 H' - L_{12} - \gamma_0 T + \omega_1) \\ -a^2(2\beta_0 H - 2\alpha_0 H' + L_{21} + \gamma_0 T + \omega_2) \end{bmatrix} = 0 \\
&L_{22} - \gamma_0 W - 2B(\alpha_0 + \beta_0) + k_2 = 0 \\
&2Ha^2 + 2H'b^2 + T = 0 \\
&2Bb^2 - 2Aa^2 + W = 0
\end{aligned} \tag{14}$$

which solve to give:

$$A=\frac{(\alpha_0+\beta_0)\,(L_{11}-k_1)-b^2\gamma_0(k_2-k_1+L_{11}+L_{22})}{2(\alpha_0+\beta_0)\,\left(\alpha_0+\beta_0-\left(a^2+b^2\right)\gamma_0\right)}$$

$$B=\frac{(\alpha_0+\beta_0)\,(L_{22}+k_2)-a^2\gamma_0(k_2-k_1+L_{11}+L_{22})}{2(\alpha_0+\beta_0)\,\left(\alpha_0+\beta_0-\left(a^2+b^2\right)\gamma_0\right)}$$

$$W=\frac{a^2(L_{11}-k_1)-b^2(L_{22}+k_2)}{\alpha_0+\beta_0-\left(a^2+b^2\right)\gamma_0}$$

$$H=\frac{\begin{bmatrix}a^2\left(L_{21}+\omega_2-2\left(\alpha_0+b^2\gamma_0\right)H'\right)\\ \\ +b^2\left(L_{12}-\omega_1+2\left(\alpha_0-b^2\gamma_0\right)H'\right)\end{bmatrix}}{2\left(a^4\gamma_0+b^2\beta_0+a^2\left(b^2\gamma_0-\beta_0\right)\right)}$$

$$T=\frac{\begin{bmatrix}2\left(a^2-b^2\right)\left(a^2\gamma_0+b^2\beta_0\right)H'\\ \\ -a^2\left(a^2(L_{21}+\omega_2)+b^2(L_{12}-\omega_1)\right)\end{bmatrix}}{a^4\gamma_0+b^2\beta_0+a^2\left(b^2\gamma_0-\beta_0\right)} \qquad (15)$$

notice that an expression has not been obtained for H'.

Next expressions for the internal and external stresses are obtained. The procedure is quite similar to that outlined in Mulchrone and Walsh (2006, Eqs. (MW62)–(MW65)) except for additional algebraic complexity due to H'. Using the values in Eq. (15) expressions for the components of stress relative to the fixed coordinate system (both internal and external) are obtained:

$$\sigma_x^{(\mathrm{i})}=P\left(\frac{\left(2\mu_\mathrm{i}k_1-p_0^{(\mathrm{i})}\right)x}{a^2}+\frac{\mu_\mathrm{i}(\omega_1-\omega_2)y}{b^2}\right)$$

$$\sigma_y^{(\mathrm{i})}=P\left(\frac{\mu_\mathrm{i}(\omega_1-\omega_2)x}{a^2}-\frac{\left(2\mu_\mathrm{i}k_2+p_0^{(\mathrm{i})}\right)y}{b^2}\right)$$

$$\sigma_x^{(\mathrm{e})}=P\left(\begin{array}{c}\dfrac{\left(2a\mu_\mathrm{e}(L_{11}-k_1)+b\left(2L_{11}\mu_\mathrm{e}-p_0^{(\mathrm{e})}\right)\right)x}{a^2b}\\ +\dfrac{\mu_\mathrm{e}\begin{pmatrix}a\left(16H'-b^2(5L_{12}+L_{21}-4\omega_1)\right)+2b^3(\omega_1-L_{12})\\ +a^3(L_{12}-3L_{21}-4\omega_2)-2a^2b(L_{12}+2L_{21}+\omega_2)\end{pmatrix}y}{ab^2\left(a^2-2ab-b^2\right)}\end{array}\right)$$

$$\sigma_y^{(\mathrm{e})}=P\left(\begin{array}{c}\dfrac{\mu_\mathrm{e}\begin{pmatrix}b(a^2(L_{12}+L_{21})-16H')+2a^3(L_{21}+\omega_2)\\ -b^3(L_{12}+L_{21})-2ab^2(L_{21}+\omega_1)\end{pmatrix}x}{ab^2\left(a^2-2ab-b^2\right)}\\ -\dfrac{\left(2b\mu_\mathrm{e}(L_{11}-k_2)+a\left(2L_{11}\mu_\mathrm{e}+p_0^{(\mathrm{e})}\right)\right)y}{ab^2}\end{array}\right) \qquad (16)$$

where the superscripts i and e refer to internal and external stress, respectively, and the subscripts x and y refer to the stress components parallel to the x and y-axes, respectively. Let the internal and external stress vectors be denoted by:

$$\boldsymbol{\sigma}^{(i)}=\begin{pmatrix}\sigma_x^{(i)}\\ \sigma_y^{(i)}\end{pmatrix}\text{ and }\boldsymbol{\sigma}^{(e)}=\begin{pmatrix}\sigma_x^{(e)}\\ \sigma_y^{(e)}\end{pmatrix}$$

These stresses are then resolved along the boundary. The boundary normal is given by Eq. (12), whereas a unit vector parallel to the boundary is given by:

$$\mathbf{s}=P\begin{pmatrix}-\dfrac{y}{b^2}\\ \dfrac{x}{a^2}\end{pmatrix} \qquad (17)$$

Therefore, the boundary normal components are:

$$\sigma_N^{(i)}=\frac{\mathbf{n}\cdot\boldsymbol{\sigma}^{(i)}}{\left|\left|\mathbf{n}\right|\right|^2}\mathbf{n} \qquad (18)$$

$$\sigma_N^{(e)}=\frac{\mathbf{n}\cdot\boldsymbol{\sigma}^{(e)}}{\left|\left|\mathbf{n}\right|\right|^2}\mathbf{n} \qquad (19)$$

and the boundary shear components are:

$$\sigma_S^{(i)}=\frac{\mathbf{s}\cdot\boldsymbol{\sigma}^{(i)}}{\left|\left|\mathbf{s}\right|\right|^2}\mathbf{s} \qquad (20)$$

$$\sigma_S^{(e)}=\frac{\mathbf{s}\cdot\boldsymbol{\sigma}^{(e)}}{\left|\left|\mathbf{s}\right|\right|^2}\mathbf{s} \qquad (21)$$

Each stress component consists of terms in x^2, y^2 and xy.

At the boundary both the normal and shear, internal and external stresses must be equal giving $\sigma_N^{(i)}=\sigma_N^{(e)}$ and $\sigma_S^{(i)}=\sigma_S^{(e)}$, each condition results in three equations (i.e. by equating like coefficients). The shear stress at the boundary is set to 0 for slip, thus a total of nine equations are to be solved. The nine equations are:

$$\frac{2a(k-L_{11})\mu_\mathrm{e}+b\left(2k\mu_\mathrm{i}+p_0^{(e)}-p_0^{(i)}-2L_{11}\mu_\mathrm{e}\right)}{ab}=0$$

$$\frac{2b(k-L_{11})\mu_\mathrm{e}+a\left(2k\mu_\mathrm{i}-p_0^{(e)}+p_0^{(i)}-2L_{11}\mu_\mathrm{e}\right)}{ab}=0$$

$$\frac{ab\mu_\mathrm{i}(\omega_2-\omega_1)+\mu_\mathrm{e}\left((bL_{12}+aL_{21})(a+b)-b^2\omega_1+a^2\omega_2\right)}{ab}=0$$

$$\frac{\mu_i(\omega_1-\omega_2)}{a}=0$$
$$\frac{\mu_i(\omega_1-\omega_2)}{b}=0$$
$$\frac{k\mu_i}{ab}=0$$
$$\frac{\left[\mu_e\begin{pmatrix}L_{12}b(a^2-b^2)+L_{21}(2a^3+a^2b-2ab^2-b^3)\\-2(8bH'+ab^2\omega_1-a^3\omega_2)\end{pmatrix}\right]}{a^4b(a^2-2ab-b^2)}$$
$$=\frac{\mu_i(\omega_1-\omega_2)}{a^4}$$
$$\frac{\left[\mu_e\begin{pmatrix}(-L_{12}+3L_{21}+4\omega_2)a^3+2b(L_{12}+2L_{21}+\omega_2)a^2+\\(b^2(5L_{12}+L_{21}-4\omega_1)-16H')a+2b^3(L_{12}-\omega_1)\end{pmatrix}\right]}{ab^4(a^2-2ba-b^2)}$$
$$=\frac{\mu_i(\omega_2-\omega_1)}{b^4}$$
$$\frac{\left((a^2+b^2)k-(a+b)^2L_{11}\right)\mu_e+2abk\mu_i}{ab}=0$$

No solution exists which satisfies all nine equations, however, omitting the equation which sets the xy-coefficient of $\sigma_S^{(i)}$ to 0 i.e. $k\mu_i/ab=0$, the following solution is obtained and letting $\mu_r=\mu_e/\mu_i$:

$$\begin{aligned}H'&=-\frac{1}{16}(a+b)^2(L_{12}+L_{21})\\k_1=k_2&=\frac{(a+b)^2L_{11}\mu_r}{2ab+(a^2+b^2)\mu_r}=k\\\omega_1=\omega_2&=\frac{aL_{21}+bL_{12}}{b-a}=\omega\\p_0^{(e)}&=-\frac{2(a^2-b^2)L_{11}\mu_i\mu_r(\mu_r-1)}{2ab+(a^2+b^2)\mu_r}+p_0^{(i)}\end{aligned}\tag{22}$$

By substituting this solution into the omitted equation, the validity of the solution can be assessed:

$$\frac{(a+b)L_{11}\mu_r\mu_i}{ab(2ab+(a^2+b^2)\mu_r)}=0\tag{23}$$

Clearly, the solution is only valid (i.e. this equation is satisfied) for (i) $\mu_r=0$, a fully rigid object or (ii) $\mu_i=0$, an area preserving void. The case of a rigid inclusion is concentrated on here so that the final solution is:

$$\begin{aligned}H'&=-\frac{1}{16}(a+b)^2(L_{12}+L_{21})\\k_1=k_2&=k=0\\\omega_1=\omega_2&=\frac{aL_{21}+bL_{12}}{b-a}=\omega\\p_0^{(e)}&=p_0^{(i)}\end{aligned}\tag{24}$$

This completes the solution.

References

Arbaret, L., Diot, H., Bouchez, J.-L., 1996. Shape fabrics of particles in low concentration suspensions: 2D analogue experiments and application to tiling in magma. Journal of Structural Geology 18, 941–950.

Arbaret, L., Mancktelow, N.S., Burg, J.-P., 2001. Effect of shape and orientation on rigid particle rotation and matrix deformation in simple shear flow. Journal of Structural Geology 23, 113–125.

Bilby, B.A., Kolbuszewski, M.L., 1975. The finite deformation of an inhomogeneity in two-dimensional slow viscous incompressible flow. Proceedings of the Royal Society of London, Series B 355, 335–353.

Bons, P.D., Barr, T.D., ten Brink, C.E., 1997. The development of *s*-clasts in non-linear viscous materials: a numerical approach. Tectonophysics 270 (1–2), 29–41.

Bose, S., Marques, F.O., 2004. Controls on the geometry of tails around rigid circular inclusions: insights from analogue modelling in simple shear. Journal of Structural Geology 26 (12), 2145–2156.

Bretherton, F.P., 1962. The motion of rigid particles in a shear flow at low Reynolds number. Journal of Fluid Mechanics 14, 284–304.

Ceriani, S., Mancktelow, N.S., Pennacchioni, G., 2003. Analogue modelling of the influence of shape and particle/matrix interface lubrication on the rotational behaviour of rigid particles in simple shear. Journal of Structural Geology 25, 2005–2021.

Eshelby, 1957. The determination of the elastic field of an ellipsoidal inclusion, and related problems. Proceedings of the Royal Society of London, Series B 241, 376–396.

Fernandez, A., 1987. Preferred orientation developed by rigid markers in two dimensional simple shear – a theoretical and experimental study. Tectonophysics 136, 151–158.

Fernandez, A., Febesse, J.L., Mezure, J.F., 1983. Theoretical and experimental study of fabrics developed by different shaped markers in two-dimensional simple shear. Bulletin de la Société géologique de France 25, 319–326.

Freeman, B., 1985. The motion of rigid ellipsoidal particles in slow flows. Tectonophysics 113, 163–183.

Ghosh, S.K., 1987. Measure of non-coaxiality. Journal of Structural Geology 9, 111–113.

Ghosh, S.K., Ramberg, H., 1976. Reorientation of inclusions by combination of pure shear and simple shear. Tectonophysics 34 (1–2), 1–70.

Herweg, M., Handy, M.R., 1998. The origin of shape preferred orientations in mylonite: inferences from in-situ experiments on polycrystalline camphor. Journal of Structural Geology 20, 681–694.

Ildefonse, B., Mancktelow, N.S., 1993. Deformation around rigid particles: the influence of slip at the particle/matrix interface. Tectonophysics 221, 345–359.

Ildefonse, B., Launeau, P., Bouchez, J.-L., Fernandez, A., 1992a. Effect of mechanical interactions on the development of shape preferred orientations: a two-dimensional experimental approach. Journal of Structural Geology 14, 73–83.

Ildefonse, B., Sokoutis, D., Mancktelow, N.S., 1992b. Mechanical interactions between rigid particles in a deforming ductile matrix. Analogue experiments in simple shear flow. Journal of Structural Geology 14, 1253–1266.

Jeffery, G.B., 1922. The motion of ellipsoidal particles immersed in a viscous fluid. Proceedings of the Royal Society of London, Series A 102, 201–211.

Jezek, J., Saic, S., Segeth, K., Schulmann, K., 1999. Three-dimensional hydrodynamical modelling of viscous flow around a rotating ellipsoidal inclusion. Computers & Geosciences 25 (5), 547–558.

Kenkmann, T., Dresen, G., 1998. Stress gradients around porphyroclasts: palaeo-piezometric estimates and numerical modelling. Journal of Structural Geology 20, 163–173.

Mancktelow, N.S., Arbaret, L., Pennacchioni, G., 2002. Experimental observations on the effect of interface slip on rotation and stabilisation of rigid particles in simple shear and a comparison with natural mylonites. Journal of Structural Geology 24, 567–585.

Mandal, N., Samanta, S.K., Chakraborty, C., 2001. Numerical modelling of heterogeneous flow fields around rigid objects with special reference to particle paths, strain shadows and foliation drag. Tectonophysics 330, 177–194.

Manga, M., 1998. Orientation distribution of microlites in obsidian. Journal of Volcanology and Geothermal Research 86, 107–115.

March, A., 1932. Mathematische Theorie der Regelung nach der Korngestalt bei affiner Deformation. Zeitschrift fur Kristallographie 81, 285–297.

Marsden, J.E., Tromba, A.J., 2003. Vector Calculus. W.H. Freeman and Company.

Marques, F.O., Bose, S., 2004. Influence of a permanent low-friction boundary on rotation and flow in rigid inclusion/viscous matrix systems from an analogue perspective. Tectonophysics 382, 229–245.

Marques, F.O., Cobbold, P.R., 1995. Development of highly non-cylindrical folds around rigid ellipsoidal inclusions in bulk simple shear regimes: natural examples and experimental modelling. Journal of Structural Geology 17, 589–602.

Marques, F.O., Coelho, S., 2001. Rotation of rigid elliptical cylinders in viscous simple shear flow: analogue experiments. Journal of Structural Geology 23, 609–617.

Marques, F.O., Coelho, S., 2003. 2-D shape preferred orientations of rigid particles in transtensional viscous flow. Journal of Structural Geology 25, 841–854.

Marques, F.O., Taborda, R., Antunes, J., 2005a. Influence of a low-viscosity layer between rigid inclusion and viscous matrix on inclusion rotation and matrix flow: a numerical study. Tectonophysics 407, 101–115.

Marques, F.O., Taborda, R., Bose, S., Antunes, J., 2005b. Effects of confinement on matrix flow around a rigid inclusion in viscous simple shear: insights from analogue and numerical modelling. Journal of Structural Geology 27, 379–396.

Mason, S.G., Manley, R. St J., 1957. Particle motion in sheared suspension: orientations and interactions of rigid rods. Proceedings of the Royal Society of London, Series A 238, 117–131.

Masuda, T., Mizuno, N., 1995. Deflection of pure shear viscous flow around a rigid spherical body. Journal of Structural Geology 17, 1615–1620.

Masuda, T., Mizuno, N., 1996a. Deflection of non-Newtonian simple shear flow around a rigid cylindrical body by the finite element method. Journal of Structural Geology 18, 1089–1100.

Masuda, T., Mizuno, N., 1996b. Computer modelling of mantled porphyroclasts in Newtonian and non-Newtonian simple shear viscous flows. Journal of Structural Geology 18, 1487–1491.

Masuda, T., Michibayashi, K., Ohta, H., 1995. Shape preferred orientation of rigid particles in a viscous matrix: reevaluation to determine kinematic parameters of ductile deformation. Journal of Structural Geology 17, 115–129.

Means, W.D., Hobbs, B.E., Lister, G.S., Williams, P.F., 1980. Vorticity and non-coaxiality in progressive deformations. Journal of Structural Geology 2, 371–378.

Mulchrone, K.F., Walsh, K., 2006. The motion of a non-rigid ellipse in a general 2D deformation. Journal of Structural Geology 28, 392–407.

Mulchrone, K.F., O'Sullivan, F., Meere, P.A., 2003. Finite strain estimation using the mean radial length of elliptical objects with confidence intervals. Journal of Structural Geology 25, 529–539.

Mushhelishvili, N.I., 1953. Some Basic Problems of the Mathematical Theory of Elasticity. Noordhoff, Groningen.

Odonne, F., 1994. Kinematic behaviour of an interface and competence contrast: analogue models with different degrees of bonding between deformable inclusions and their matrix. Journal of Structural Geology 16, 997–1006.

Passchier, C.W., 1987. Stable positions of rigid objects in non-coaxial flow – a study in vorticity analysis. Journal of Structural Geology 19, 113–127.

Passchier, C.W., Simpson, C., 1986. Porphyroclast systems as kinematic indicators. Journal of Structural Geology 8, 831–843.

Passchier, C.W., Sokoutis, D., 1993. Experimental modelling of mantled porphyroclasts. Journal of Structural Geology 15, 895–909.

Passchier, C.W., ten Brink, C.E., Bons, P.D., Sokoutis, D., 1993. δ Objects as a gauge for stress sensitivity of strain in mylonites. Earth and Planetary Science Letters 120, 239–245.

Passchier, C.W., Trouw, R.A.J., 1996. Microtectonics. Springer, Berlin.

Pennacchioni, G., Di Toro, G., Mancktelow, N.S., 2001. Strain-insensitive preferred orientation of porphyroclasts in Mont Mary mylonites. Journal of Structural Geology 23, 1281–1298.

Pennacchioni, G., Fasolo, L., Cecchi, M.M., Salasnich, L., 2000. Finite-element modeling of simple shear flow in Newtonian and non-Newtonian fluids around circular rigid particle. Journal of Structural Geology 22, 683–692.

Samanta, S.K., Bhattacharyya, G., 2003. Modes of detachment at the inclusion–matrix interface. Journal of Structural Geology 25, 1107–1120.

Samanta, S.K., Mandal, N., Chakraborty, C., 2003. Flow patterns around rigid inclusions in a multiple inclusion system undergoing bulk simple shear deformation. Journal of Structural Geology 25, 209–221.

Schmid, D.W., 2002. Finite and infinite heterogeneities under pure and simple shear, Unpublished Thesis, ETH, Zurich.

Schmid, D.W., Podladchikov, Y.Y., 2003. Analytical solutions for deformable elliptical inclusions in general shear. Geophysical Journal International 155, 269–288.

Schmid, D.W., Podladchikov, Y.Y., 2004. Are isolated stable rigid clasts in shear zones equivalent to voids? Tectonophysics 384, 233–242.

Schmid, D.W., Podladchikov, Y.Y., 2005. Mantled porphyroblast gauges. Journal of Structural Geology 27, 571–585.

Taborda, R., Antunes, J., Marques, F.O., 2004. 2-D rotation behavior of a rigid ellipse in confined viscous simple shear: numerical experiments using FEM. Tectonophysics 379, 127–137.

ten Brink, C.E., Passchier, C.W., 1995. Modelling of mantled porphyroblasts using non-Newtonian rock analogue materials. Journal of Structural Geology 17, 131–146.

Van Den Driessche, J., Brun, J.P., 1987. Rolling structures at large shear strain. Journal of Structural Geology 9 (5–6), 691–704.

Xypolias, P., Koukouvelas, I.K., 2001. Kinematic vorticity and strain rate patterns associated with ductile extrusion in the Chelmos Shear Zone (External Hellenides, Greece). Tectonophysics 338, 59–77.